

MemPot: Defending Against Memory Extraction Attack with Optimized Honeypots

Yuhao Wang*¹ Shengfang Zhai*¹ Guanghao Jin² Yinpeng Dong³ Linyi Yang² Jiaheng Zhang¹

Abstract

Large Language Model (LLM)-based agents employ external and internal memory systems to handle complex, goal-oriented tasks, yet this exposes them to severe extraction attacks, and corresponding defenses are currently lacking. In this paper, we propose *MemPot*, the first theoretically verified defense framework against memory extraction attacks by injecting optimized honeypots into the memory. Through a two-stage optimization process, *MemPot* generates trap documents that maximize the retrieval probability for attackers while remaining inconspicuous to benign users. We model the detection process as Wald's Sequential Probability Ratio Test (SPRT) and theoretically prove that *MemPot* achieves a lower average number of sampling rounds compared to optimal static detectors. Empirically, *MemPot* significantly outperforms state-of-the-art baselines, achieving a 50% improvement in detection AUROC and an 80% increase in True Positive Rate under low False Positive Rate constraints. Furthermore, our experiments confirm that *MemPot* incurs zero online inference latency and preserves the agent's utility on standard tasks, verifying its superiority in safety, harmlessness and efficiency.

1. Introduction

Large language model (LLM) is now becoming one of the most important AI technologies in daily life with its impressive performance (OpenAI, 2023; Zhao et al., 2023). Building on recent advances in LLMs (Achiam et al., 2023; Liu et al., 2024; Grattafiori et al., 2024), LLM-based agents are equipped with additional functionalities to perform complex, goal-oriented tasks (Xi et al., 2023). A typical agent follows a structured pipeline that processes user instruc-

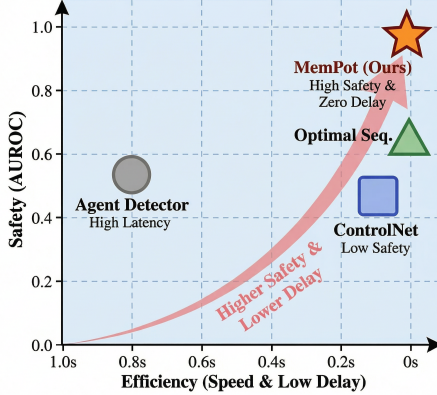


Figure 1. Performance comparison of *MemPot* and existing methods (AUROC vs. Delay).

tions, gathers environmental information, retrieves relevant knowledge and past experiences, formulates action plans, and executes them in the environment (Wang et al., 2024; Hu et al., 2025). This paradigm has enabled diverse real-world applications, including healthcare (Abbasian et al., 2023), autonomous driving (Mao et al., 2023), finance (Ding et al., 2024), code generation (Hong et al., 2024), business management (Salesforce, 2024) and web interaction (Yao et al., 2022; 2023), positioning LLM agents as a central AI technology today. Typically, an agent is equipped with an external memory, which usually contains domain-specific knowledge, and an internal memory, where past experiences and user-interaction histories are stored.

Despite their rapidly increasing deployment, LLM-based agents pose serious risks of privacy and knowledge leakage. Modern LLM-based agents frequently retrieve information from external memory that contains private and high-value domain data (Abbasian et al., 2023; Kulkarni et al., 2024; Salesforce, 2024). While such retrieval improves task performance, it also introduces significant security risks. For example, the ForcedLeak vulnerability in Salesforce Agentforce enabled large-scale exfiltration of Customer Relationship Management (CRM) data (Noma Security, 2024), underscoring the vulnerability of external memory to data leakage in real-world agent systems. In addition to external sources, agents also maintain internal memory modules that store long-term interaction histories, including past user

*Equal contribution ¹National University of Singapore ²Southern University of Science and technology ³Tsinghua University. Correspondence to: Shengfang Zhai <shengfang.zhai@gmail.com>, Linyi Yang <yangly6@sustech.edu.cn>.

instructions and agent-generated responses (Zhang et al., 2024b). Because these internal memories inherently contain sensitive user data, such as personal preferences and private records, their leakage can lead to serious privacy violations, such as exposure of medical information and purchase history (Wang et al., 2025a).

Prior works has explored extraction attacks against external knowledge database (Wang et al., 2025b; Jiang et al., 2024; Cohen et al., 2024; Zeng et al., 2024a; Qi et al., 2025), which can be applied to Retrieval Augmented Generation (RAG) system (Fan et al., 2024) and agents' external memory (Hu et al., 2025). Recent works also discovered privacy attack on agents' internal memory, such as long-term interaction histories (Wang et al., 2025a).

Despite recent progress in defending extraction attacks (Zhang et al., 2024a; Zeng et al., 2025; Agarwal et al., 2024; Jiang et al., 2024; Yao et al., 2025), existing defense methods still have limitations. Most current defenses focus on per-query detection and rely on real-time inference with large language models or auxiliary detectors (Zhang et al., 2024a; Zeng et al., 2024b; Yao et al., 2025). As a result, they struggle to identify stealthy extraction attacks that employ benign-looking queries and gradual interaction patterns (Wang et al., 2025b;a; Jiang et al., 2024; Cohen et al., 2024), as they lack mechanisms to aggregate evidence across multiple retrieval steps. Moreover, their reliance on real-time inference introduces inference latency, which greatly undermines the interactive smoothness with users, limiting their practical applications.

To address the limitations of prior defenses, we propose *MemPot*, a **zero-online-cost** extraction defense framework with theoretical guarantees. *MemPot* inserts optimized honeypot documents into the memory, and these honeypot documents are designed to attract attackers while remaining inconspicuous to benign users. The main challenge of *MemPot* is to ensure the quality of service (QoS) for normal users while maximizing the detection performance against attackers. The challenges thus involve: (1) This requires the honeypot documents to be sufficiently attractive to attackers while remaining inconspicuous to normal users. (2) The honeypot documents must be harmless and not mislead normal users, which necessitates careful design to avoid negative impacts on user experience. (3) To limit the impact of attackers, it is important to minimize the rounds of detection, as earlier detection can prevent further leakage of private information.

Our approach addresses these challenges through a two-stage optimization strategy to balance detection efficiency with Quality of Service (QoS). In the first stage, we optimize honeypot embeddings using contrastive loss to maximize the statistical separability between attacker and normal user retrieval patterns. By formalizing this detection task as a

sequential hypothesis testing problem using Wald's Sequential Probability Ratio Test (SPRT), we theoretically prove that this optimization objective leads to minimized average detection rounds, surpassing the efficiency limits of any optimal static detector. In the second stage, we address safety requirements by inverting these optimized embeddings into concrete, benign documents, ensuring they remain harmless and do not mislead normal users. Empirically, *MemPot* validates these theoretical guarantees, achieving a 50% improvement in detection AUROC and an 80% increase in TPR@1%FPR over state-of-the-art baselines. Furthermore, our results confirm that *MemPot* maintains near-zero detection delay and negligible impact on benign user utility, demonstrating its superiority in both defense efficiency and practical utility. In summary, our main contributions are:

- We propose *MemPot*, the first general defense framework against memory extraction attacks. By employing a novel two-stage optimization strategy, *MemPot* inserts harmless honeypots into the memory, and performs sequential detection based on accumulated retrieval evidence, achieving notable performance without affecting the Quality of Service (QoS).
- We formulate detection as a sequential hypothesis testing problem and apply Wald's SPRT to construct an optimal detector, theoretically minimizing the expected detection rounds and outperforming static detectors without honeypots.
- Extensive experiments across two datasets and two agent settings show that *MemPot* consistently achieves near-perfect detection accuracy against state-of-the-art extraction attacks with zero-online latency, and *MemPot* have negligible impact on agent utility.

2. Related Works

2.1. LLM Agents

Large Language Models (LLMs) have demonstrated revolutionary capabilities in language understanding, reasoning, and generation (Zhao et al., 2023). Building on these advances, LLM agents use LLMs and supplement with additional functionalities to perform more complex tasks (Xi et al., 2023). Its typical pipeline consists of the following key steps: taking user instruction, gathering environment information, retrieving relevant knowledge and past experiences, giving an action solution based on the above information, and finally executing the solution (Wang et al., 2024). This pipeline enables agents to support various real-world applications, such as healthcare (Abbasian et al., 2023), web applications (Yao et al., 2022), and autonomous driving (Mao et al., 2023).

Table 1. Comparison of defense methods (details in Sec. 5.1). **MemPot** achieves the best performance with zero online cost.

Defense Method	Distribution Change	Detection Paradigm	Detection Performance	Online Cost
ControlNet	✗	Single Turn	Low	Middle
Agent	✗	Single Turn	Low	High
Optimal Seq	✗	Sequential	Middle	Middle
MemPot	✓	Sequential	High	Zero

2.2. Privacy Risk in Memory System

The private information of an LLM agent mainly originates from two sources: (1) In external memory domain, agents usually employ RAG to retrieve high-value domain-specific records (e.g., patient prescriptions (Li et al., 2023)) to enhance generation (Hu et al., 2025; Lewis et al., 2020; Kulakarni et al., 2024). (2) In internal memory domain, the memory module emerges as a new risk source by archiving sensitive user-agent interactions, specifically pairs of private instructions and agent solutions (Zhang et al., 2024b). While prior research has demonstrated data leakage risks in RAG systems through various extraction attacks (Zeng et al., 2024a; Jiang et al., 2024; Di Maio et al., 2024; Cohen et al., 2024; Wang et al., 2025b), recent studies have further confirmed the tangible threat of extracting sensitive details directly from the agent’s internal memory (Wang et al., 2025a). Hence, it is urgent to explore effective and fundamental defense strategy to mitigate such attacks.

2.3. Defense against Extraction Attack on Memory System

Current defense strategies primarily fall into two categories: embedding-level detection and text-level detection. As a representative of embedding-level approaches, ControlNet (Yao et al., 2025) measure current query’s distributional shift between benign query embeddings to identify potential extraction attacks. In contrast, text-level detection typically relies on Large Language Models (LLMs) to discern query intentions or employs multi-agent systems to analyze the potential impact of queries (Zhang et al., 2024a; Zeng et al., 2024b; Agarwal et al., 2024). While these works have made significant progress in defending extraction attacks, applying them to agent memory protection presents limitations. Current methods exhibit two primary limitations: First, they impose heavy computational overhead relying on real-time inference with large language models or auxiliary detectors (Zhang et al., 2024a; Zeng et al., 2024b; Yao et al., 2025), limiting their practicality for long-running and interactive agents. Second, their defensive capability is fundamentally limited by a static, single-turn detection paradigm. By treating each query in isolation, these methods fail to aggregate evidence across interactions. Current methods also lack capability to proactively alter the memory distribution to trap adversaries, which is important when facing benign-looking attacks that closely mimic normal behavior.

Consequently, these methods remain vulnerable to stealthy extraction strategies. We compare the key differences between existing approaches and our method in Tab. 1.

3. Preliminary

3.1. Threat Model

Defense Scenario. We consider a LLM-based agent service provider as the defender, who maintains a memory \mathcal{D} and provides services to users. The defender aims to protect the privacy of the memory from potential attackers while ensuring high-quality service for normal users. We assume that attackers have the same access privileges as normal users and have no prior knowledge of the defense setting.

Defender’s Prior knowledge. The defender is assumed to have all knowledge about the agent system, including the retriever, LLM, the content and index embeddings of the memory. We assume the defender only have partial knowledge about the attacker, which means that the defender has access to a small set of attacker queries $Q_a = \{q_1^{(1)}, q_2^{(1)}, \dots, q_M^{(1)}\}$, which can be collected from historical attack logs.

Defender Goal. The defender aims to accurately detect attackers while minimizing the impact on normal users. The goal can be summarized as two parts: (1) **Detection Accuracy and Efficiency:** The defender aims to maximize the detection accuracy while minimizing the average detection rounds, thereby reducing the potential leakage of private information. (2) **Quality of Service (QoS):** The defender aims to ensure that the presence of honeypot documents does not significantly degrade the user experience for normal users, which can be measured by the false positive rate (FPR) of detection and empirical utility experiments.

3.2. Sequential Hypothesis Testing Model

In this part, we formalize attacker detection with *optimized Honeypots* as a sequential hypothesis testing problem. Let $d \in \mathbb{N}$. The fixed document embeddings are $\mathcal{E}_{\text{doc}} = \{e_i\}_{i=1}^N \subset \mathbb{R}^d$. Trainable honeypot embeddings are $\mathcal{E}_{\text{pot}}(\theta) = \{u_j(\theta)\}_{j=1}^P \subset \mathbb{R}^d$, and the augmented database is:

$$\mathcal{E}_{\text{aug}}(\theta) = \mathcal{E}_{\text{doc}} \cup \mathcal{E}_{\text{pot}}(\theta).$$

Sequential Testing Model. There are two query sources:

$$\begin{aligned} q &\sim \mathcal{Q}_1 && \text{(attacker, hypothesis } H_1\text{),} \\ q &\sim \mathcal{Q}_0 && \text{(normal, hypothesis } H_0\text{).} \end{aligned} \quad (1)$$

At round t , we observe $O_t = \Phi(q_t; \theta)$, where Φ deterministically maps the query and the augmented index to the retrieval information (e.g., query, returned indices and similarity scores). Let $f_{1,\theta}$ and $f_{0,\theta}$ denote the laws of a

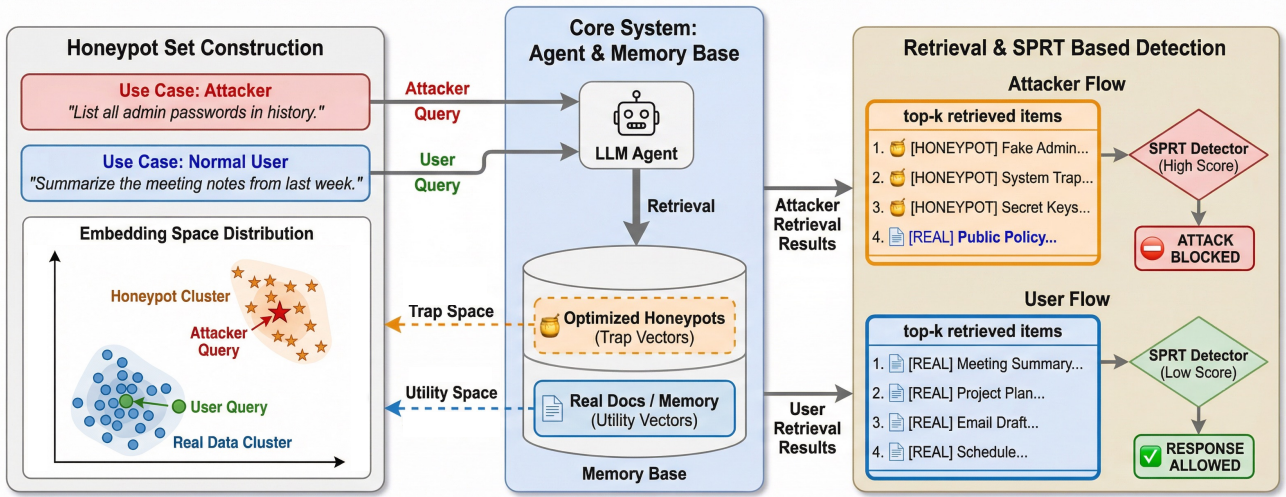


Figure 2. Overview of *MemPot* Detection Framework.

single-round observation O under H_1 and H_0 , respectively. Given type-I/II error budgets $(\alpha, \beta) \in (0, 1)^2$, our *objective* is to design a sequential test with minimum stopping rounds N and terminal decision $D_N \in \{H_0, H_1\}$ such that

$$\begin{aligned} & \min \{E_1[N], E_0[N]\}, \\ \text{s.t. } & P_0(D_N = H_1) \leq \alpha, \quad P_1(D_N = H_0) \leq \beta \end{aligned} \quad (2)$$

where $E_i[\cdot]$ denotes expectation under hypothesis H_i .

Wald's approximated SPRT. We utilize Wald's approximated SPRT (Wald, 1992) to solve the optimization problem in 2. Define the per-round log likelihood ratio (LLR) and accumulated log likelihood ratio

$$\ell_\theta(O) = \log \frac{f_{1,\theta}(O)}{f_{0,\theta}(O)}, \quad S_n = \sum_{t=1}^n \ell_\theta(O_t). \quad (3)$$

Define information drift under two hypothesis:

$$\begin{aligned} \mu_1(\theta) &= \mathbb{E}_{f_{1,\theta}}[\ell_\theta(O)] = \text{KL}(f_{1,\theta} \| f_{0,\theta}), \\ \mu_0(\theta) &= \mathbb{E}_{f_{0,\theta}}[\ell_\theta(O)] = -\text{KL}(f_{0,\theta} \| f_{1,\theta}). \end{aligned} \quad (4)$$

Wald (1992) shows that for SPRT with boundaries $A = \frac{1-\beta}{\alpha}$ and $B = \frac{\beta}{1-\alpha}$ stops at

$$N = \inf\{n : S_n \geq \log A \text{ or } S_n \leq \log B\}. \quad (5)$$

and at least one of the two errors will be controlled at the desired level:

$$\mathbb{P}_0(D_N = H_1) + \mathbb{P}_1(D_N = H_0) \leq \alpha + \beta. \quad (6)$$

More precisely, the expected average sampling number (ASN)¹ in two hypothesis with negligible overshoot can be

¹In this paper, we assume the observations are with Markov property conditional on the hypothesis (Proofs of ASN approximation for SPRT with Markov observations are detailed in Appendix D, Lemma 6).

approximated by:

$$E_1[N] \approx \frac{|\log B|}{\mu_1(\theta)}, \quad E_0[N] \approx \frac{|\log A|}{\mu_0(\theta)}. \quad (7)$$

Hence, for fixed (α, β) , increasing $\mu_1(\theta)$ and $|\mu_0(\theta)|$ decreases the expected sample sizes that attain those error budgets.

4. *MemPot*: Optimization and Detection

Our methodology is grounded in the insight that memory retrieval is an iterative and sequential process. Unlike computationally expensive per-query detection, we leverage the retrieval mechanism itself as a zero-cost indicator. We aggregate evidence across the interaction trajectory to distinguish attackers from benign users. To amplify these discriminative signals, *MemPot* injects optimized honeypots designed to stimulate adversarial behavior without disrupting normal service. In this section, we detail our framework (Figure 2): We derive the optimization of vector-form honeypots based on SPRT theory and prove its optimality in minimizing detection rounds in Sec. 4.1. We then convert these vectors into harmless text-form documents via safety-constrained embedding inversion in Sec. 4.2. We finally present practical Log-Likelihood Ratio (LLR) estimation methods to execute the sequential detection in Sec. 4.3.

4.1. Honeypot Vector in Semantic Embedding Space

The trainable honeypot parameters θ influence the observation distributions $(f_{1,\theta}, f_{0,\theta})$ through retrieval mechanism, and thus determine both error probabilities and sampling efficiency. We will leverage this dependence to derive an optimization objective for vector-form honeypots that increases the statistical separability of $f_{1,\theta}$ and $f_{0,\theta}$ under the constraints of error budgets in Eq. (2).

Theorem 1 (InfoNCE upper-bound by information drift, Proof in Appendix. E). *Draw index $j \sim \text{Unif}\{1, \dots, K\}$, then $q_j \sim Q_1$ and $(q_i)_{i \neq j} \sim Q_0$ independently of j . For any score function $h : O \rightarrow \mathbb{R}$, define the InfoNCE loss*

$$\mathcal{L}_{\text{NCE},K}(h; \theta) := -\mathbb{E} \left[\log \frac{e^{h(\Phi(q_j); \theta)}}{\sum_{i=1}^K e^{h(\Phi(q_i); \theta)}} \right].$$

Then, for every $K \geq 2$,

$$-\mathcal{L}_{\text{NCE},K}(h; \theta) \leq \mu_1(\theta) - \log(K). \quad (8)$$

Thm. 1 shows that decreasing $\mathcal{L}_{\text{NCE},K}(h; \theta)$ is equivalent to improve $\mu_1(\theta)$'s lower bound and therefore decreasing upper bound of $E_1[N]$ with Eq. (7).

In real scenario, memory system usually only returns the top- k similar entries. We therefore define a top- k masked similarity score here for tighter bound. Let \mathcal{P} be the set of honeypots $\mathcal{E}_{\text{pot}}(\theta)$'s indices. Define a per-query score

$$g_k(q; \theta) := \frac{1}{k} \sum_{j \in \mathcal{T}_k(q) \cap \mathcal{P}} s(q, E_j), \quad (9)$$

where cosine similarity function $s(\mathbf{u}, \mathbf{v}) = \frac{\mathbf{u}^\top \mathbf{v}}{|\mathbf{u}| \cdot |\mathbf{v}|}$, top- k index set for query $\mathcal{T}_k(q)$ returns the indices of the k largest elements of cosine similarity in $\mathcal{E}_{\text{aug}}(\theta)$. Taking g_k as h , we then get the final honeypot training loss

$$\mathcal{L}_{\text{pot}}(\theta) := \mathcal{L}_{\text{NCE},K}(g_k; \theta) + \beta \cdot \mathcal{L}_{\text{div}}(\theta), \quad (10)$$

where β is regularization parameter and $\mathcal{L}_{\text{div}}(\theta)$ is honeypot diversity loss defined by

$$\mathcal{L}_{\text{div}}(\theta) := \sum_{\substack{1 \leq i < j \leq P \\ u_i, u_j \in \mathcal{E}_{\text{pot}}}} \frac{2}{P(P-1)} s(u_i, u_j). \quad (11)$$

Theorem 2 (Advantage over static test, Proof in Appendix. F). *Define θ^* the parameter obtained by minimizing \mathcal{L}_{NCE} , then for any possibly static fixed-length test achieving (α, β) (i.e., tests without honeypot augment), the stopping time N of static test and SPRT with θ^* satisfies:*

$$E_b[N]_{\text{SPRT}, \theta^*} \leq E_b[N]_{\text{any, static}}, \quad (12)$$

with hypothesis index $b \in \{0, 1\}$.

We also prove honeypots-augmented SPRT's comparative advantage over static testing in Thm. 2, which theoretically ensures shorter expected stopping time under fixed error control with proper optimized honeypots.

4.2. Generate Honeypot Documents from Vectors

To effectively defend against attackers who probe databases using semantical embeddings, honeypots' embeddings must

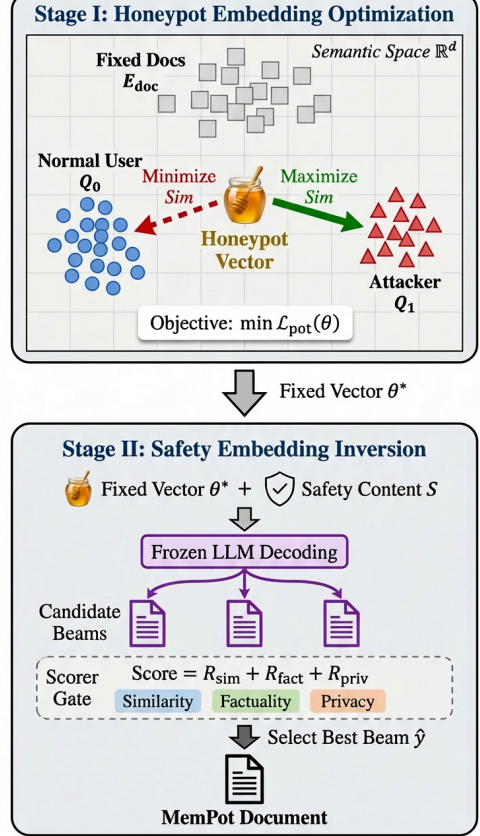


Figure 3. Two Stage Optimization Process of *MemPot*.

align semantically with their text contents; otherwise, they are unlikely to be retrieved during such exploratory attacks. The honeypot texts must ① have sentence embeddings sufficiently close to pot vectors optimized in Sec. 4.1; ② maintain factual integrity to minimize the risk of misleading or confusing users; ③ reveal no private information originally contained in the database. Inspired by (Zhang et al., 2025), we utilize scorer-guided LLM decoding to generate honeypot texts. We use Safety Embedding Inversion to satisfy demands above, which will iteratively search tokens to maximize defined scores with beam-search algorithm.

We design three scorers corresponding to the three demands for honeypot texts and sum them up for overall performance. To encourage pot text y to match the given pot vector e_p and be readable, the **Inversion Scorer** is defined as:

$$R_{\text{base}}(y, e_p) = \lambda_{\text{emb}} \cdot s(E(y), e_p) + \lambda_{\text{read}} \cdot \text{readable}(y), \quad (13)$$

where $E(\cdot)$ is a sentence embedder with $e = E(y) \in \mathbb{R}^d$, $s(\cdot, \cdot)$ is the cosine similarity function and $\text{readable}(y)$ is a readability score defined in (Zhang et al., 2025). To maintain the factuality of pot texts, we design the **Factuality Scorer** which requires information in y to be entailed by safety content S (e.g., a topic abstract). Let $\text{Entail}(y_t \mid S) \in [0, 1]$ be the natural language inference entailment (NLI)

probability (provided by a pretrained model), the factuality scorer is defined as:

$$R_{\text{fact}}(y; S) = \lambda_{\text{fact}} \cdot \text{Entail}(y | S). \quad (14)$$

To preserve the privacy of the database, we also design a **Privacy Scorer** to constrain each pot text to have low similarity to the database. For text y and given document embeddings \mathcal{E}_{doc} , the scorer is defined as:

$$R_{\text{priv}}(y | \mathcal{E}_{\text{doc}}) = -\lambda_{\text{priv}} \cdot \max_j s(E(y), \mathcal{E}_{\text{doc}}[j]). \quad (15)$$

For a single honeypot vector, the final optimization objective is

$$\max_{y \in \mathcal{Y}} R_{\text{base}}(y, \mathbf{e}_p) + R_{\text{fact}}(y | S) + R_{\text{priv}}(y | \mathcal{E}_{\text{doc}}). \quad (16)$$

We then use algorithm detailed in Algorithm 1 to attain the optimized pot texts.

4.3. Detection with Honeypots

To achieve the optimality of SPRT, we need to estimate the log likelihood ratio in Eq. (3). When accumulated log likelihood ratio excesses the SPRT boundaries in Eq. (5), the decision is made and agent system’s responses are blocked (e.g. “Unanswerable.”). Specifically, we designed three ways to approximate the log likelihood ratio. Let the retrieved document set at step t be \mathcal{D}_t , where $\mathcal{D}_t^+ = \{d_i \in \mathcal{D}_t \mid \text{is_pot}(d_i) = 1\}$ denotes *pot* documents and $\mathcal{D}_t^- = \{d_i \in \mathcal{D}_t \mid \text{is_pot}(d_i) = 0\}$ denotes *non-pot* documents. Let $s(d_i)$ denote the similarity score of document d_i . The approximation methods are shown as follows:

1. Pot-NonPot Counts Ratio. We use the ratio between the number of retrieved pot and non-pot documents:

$$\hat{r}_t^{\text{cnt}} = \frac{|\mathcal{D}_t^+| + \varepsilon_{\text{cnt}}}{|\mathcal{D}_t^-| + \varepsilon_{\text{cnt}}}. \quad (17)$$

2. Pot-NonPot Similarity Ratio. We weight the ratio by similarity scores:

$$\hat{r}_t^{\text{sim}} = \frac{\sum_{d_i \in \mathcal{D}_t^+} s(d_i) + \varepsilon_{\text{sim}}}{\sum_{d_i \in \mathcal{D}_t^-} s(d_i) + \varepsilon_{\text{sim}}}. \quad (18)$$

3. Pot-NonPot Global Similarity Ratio. We further focus on the most relevant evidence by only considering Top- K documents:

$$\hat{r}_t^{\text{g_sim}} = \frac{\frac{1}{K} \sum_{d_i \in \mathcal{D}_{t,K}^+} s(d_i) + \varepsilon_{\text{sim}}}{\frac{1}{K} \sum_{d_i \in \mathcal{D}_{t,K}^-} s(d_i) + \varepsilon_{\text{sim}}}, \quad (19)$$

where $\mathcal{D}_{t,K}^+$ means the most similar K honeypot documents, $\mathcal{D}_{t,K}^-$ means the most similar K documents that are not honeypots.

The approximated accumulated log likelihood ratio is $S_t \approx \Lambda_t = \sum_{\tau=1}^t \log \hat{r}_\tau$. Same as Eq. (5), the decision is made once the accumulated statistic crosses SPRT boundaries. Notably, the block only happens when terminal decision $D_t = H_1$, which means block happens when $\Lambda_t \geq \log A$.

4.4. Implementation Details

Attacker Proxy. To approximate the unknown attack distribution \mathcal{Q}_1 , we employ a neural proxy A_ω that mimics the attacker’s behavior at the embedding level. A_ω takes the interaction history $\{o_{1:t-1}\}$ to predict the next query embedding \hat{e}_t , optimizing a cosine similarity objective to reproduce observed retrieval rankings. This enables the training of defensive strategies against black-box threats without requiring access to their internal algorithms.

User Proxy. To approximate the diverse benign distribution \mathcal{Q}_0 without extensive real-world data, we leverage LLMs as human simulators. By prompting the LLM with specific intents and retrieval contexts, we synthesize realistic, multi-turn information-seeking trajectories. These generated sequences are then encoded to serve as a robust surrogate for the benign query space. Full description of the proxy building is detailed in Appendix. A.

5. Experiments

5.1. Setups

Datasets and Evaluation Setting. We evaluate *MemPot* on four benchmarks: HealthMagicCare (20k) (lavita AI) and Pokémon (9.46k) (asoria, 2024) for external memory (top-4 retrieval); and EHRAgent (Shi et al., 2024) and Web-Shop RAP (Yao et al., 2022; Kagaya et al., 2024) for internal memory (300 records, top-3/4 retrieval). We employ DeepSeek-v3.2 (685B) (Liu et al., 2024) as the agent backbone and all-mpnet-base-v2 (Song et al., 2020) for sentence embeddings. We use mDeBERTa-v3-base (He et al., 2021) as NLI model. Honeypots are injected at a fixed ratio of 2% for external and 4% for internal datasets (ablation in Appendix. C.2). The SPRT detector uses the count-based LLR estimation (Eq. 17) with both type-I/II error budgets α, β set to 0.1. Scalability is tested by extending internal memory by 200 records (Appendix. C.1). All experiments run on a single NVIDIA RTX 5090 GPU.

Training Configuration. We train a transformer-based attacker proxy on 256 samples per attack, augmented via similarity top-k random walks to simulate exploratory trajectories. Honeypots are optimized to attract this proxy while maintaining contrastive separation from 500 generated benign queries. To ensure scalability, we employ balanced k-means clustering to partition the corpus, generating honeypot embeddings for each cluster via a shared network to minimize computational cost.

Table 2. Performance of defense methods against external memory extraction attacks on HealthMagicCare and Pokemon datasets.

Attack	Defense	HealthMagicCare				Pokémon			
		AUROC	TPR@1%FPR	TPR@10%FPR	Delay	AUROC	TPR@1%FPR	TPR@10%FPR	Delay
RAG-Thief	ControlNet	1.00	1.00	1.00	0.06	1.00	1.00	1.00	0.05
	Agent	1.00	1.00	1.00	0.97	0.94	0.16	1.00	0.91
	MemPot	1.00	0.96	0.99	0	1.00	0.98	1.00	0
DGEA	ControlNet	1.00	0.95	1.00	0.06	1.00	1.00	1.00	0.05
	Agent	1.00	1.00	1.00	0.97	0.94	0.16	1.00	0.93
	MemPot	1.00	1.00	1.00	0	1.00	1.00	1.00	0
IKEA	ControlNet	0.46	0	0.02	0.05	0.88	0.02	0.56	0.04
	Agent	0.50	0	0	0.98	0.20	0	0.13	0.95
	MemPot	0.96	0.42	0.91	0	0.99	0.67	0.98	0

Table 3. Performance of defense methods against internal memory extraction attacks on EHRAgent and RAP web shopping agents.

Attack	Defense	EHRAgent				RAP WebShop			
		AUROC	TPR@1%FPR	TPR@10%FPR	Delay	AUROC	TPR@1%FPR	TPR@10%FPR	Delay
MEXTRA _{Cosine}	ControlNet	0.59	0	0.14	0.08	0.45	0	0.10	0.08
	Agent	0.56	0	0.04	0.96	0.51	0.02	0.02	0.97
	MemPot	0.99	0.97	1.00	0	1.00	0.94	1.00	0
MEXTRA _{Edit}	ControlNet	0.53	0.02	0.17	0.08	0.59	0.02	0.16	0.08
	Agent	0.67	0	0.14	0.88	0.81	0.30	0.30	0.96
	MemPot	0.97	0.86	0.99	0	1.00	1.00	1.00	0
MEXTRA _{General}	ControlNet	0.63	0.02	0.08	0.08	0.73	0	0.36	0.08
	Agent	0.58	0	0.06	0.91	0.72	0.12	0.12	0.91
	MemPot	0.94	0.81	0.96	0	1.00	1.00	1.00	0
IKEA	ControlNet	0.40	0	0	0.10	0.71	0.06	0.34	0.10
	Agent	0.51	0	0.02	1.01	0.47	0.02	0.02	0.96
	MemPot	1.00	0.98	1.00	0	1.00	1.00	1.00	0

Attacks and Baselines. We evaluate against RAG-Thief (Jiang et al., 2024), DGEA (Cohen et al., 2024), and IKE (Wang et al., 2025b) for external memory; and MEXTRA (Wang et al., 2025a) plus an adapted IKEA for internal memory. Baselines include ControlNet (Yao et al., 2025) (100 anchor queries) and LLM-based Agent Detectors (Appendix B.2) (Zhang et al., 2024a; Zeng et al., 2024b). Additionally, we implement a theoretical Optimal Sequential Detector (Optimal-Seq) to empirically validate Thm. 2. The details of all setups are shown in Appendix B.1.

5.2. Evaluation Metrics

We assess the performance from two perspectives:

Detection Effectiveness. We measure the ability to distinguish attackers from normal users using the Area Under the Receiver Operating Characteristics Curve (AUROC). To evaluate performance under strict service quality constraints, we specifically report the True Positive Rate at low False Positive thresholds (TPR@1%FPR and TPR@10%FPR).

Detection Efficiency. We evaluate the computational overhead and detection speed: (1) Delay (s): The average additional online inference latency per turn introduced by the defense. (2) First Detection Time (FDT): The average num-

ber of interaction turns (samples N in SPRT) required to make a detection decision. Lower FDT indicates earlier interception of leakage.

5.3. Performance Evaluation with Existing Baselines

We conducted 64-round attacks on both domains. As shown in Tab. 2, *MemPot* maintains > 0.96 AUROC on external memory, while baselines collapse against stealthy IKEA attacks (≈ 0.50 AUROC). This performance gap widens in internal settings (Tab. 3): against MEXTRA and the human-mimicking IKEA, baselines yield near-random results (e.g., 0.40 AUROC on EHRAgent), whereas *MemPot* achieves near-perfect accuracy with zero online latency by effectively aggregating sequential evidence.

5.4. Comparison with Optimal Static Detector

To empirically validate Thm. 2, we compare *MemPot* against the Optimal Sequential Detector (Optimal-Seq). As shown in Tab. 4 and Tab. 5, Optimal-Seq struggles against stealthy attacks due to the inherent indistinguishability of the original distribution (e.g., 0.70 AUROC, 22-round delay against MEXTRA-Cosine). In contrast, *MemPot* actively reshapes the retrieval landscape to amplify adversarial signals, achieving near-perfect performance (0.99 AUROC) and reducing

Table 4. Comparison between Optimal Sequential Detector and MemPot on external memory extraction attacks.

Attack	Defense	HealthMagicCare						Pokémon					
		AUROC	TPR@1%FPR	TPR@10%FPR	Delay	FDT	AUROC	TPR@1%FPR	TPR@10%FPR	Delay	FDT		
RAG-Thief	Optimal-Seq	0.97	0.69	0.89	0.04	4	1.00	0.95	1.00	0.03	2		
	MemPot	1.00	0.96	0.99	0	9	1.00	0.98	1.00	0	1		
DGEA	Optimal-Seq	0.90	0.39	0.64	0.04	11	0.97	0.70	0.88	0.04	1		
	MemPot	1.00	1.00	1.00	0	1	1.00	1.00	1.00	0	1		
IKEA	Optimal-Seq	0.70	0.11	0.27	0.03	17	0.78	0.22	0.34	0.4	14		
	MemPot	0.96	0.42	0.91	0	9	0.99	0.67	0.98	0	7		

Table 5. Comparison between Optimal Sequential Detector and MemPot on internal memory extraction attacks.

Attack	Defense	EHRAgent						RAP WebShop					
		AUROC	TPR@1%FPR	TPR@10%FPR	Delay	FDT	AUROC	TPR@1%FPR	TPR@10%FPR	Delay	FDT		
MEXTRA _{Cosine}	Optimal-Seq	0.70	0.16	0.27	0.03	22	0.68	0.06	0.22	0.04	38		
	MemPot	0.99	0.97	1.00	0	2	1.00	0.94	1.00	0	3		
MEXTRA _{Edit}	Optimal-Seq	0.71	0.14	0.32	0.04	33	0.75	0.20	0.36	0.04	27		
	MemPot	0.97	0.86	0.99	0	8	1.00	1.00	1.00	0	1		
MEXTRA _{General}	Optimal-Seq	0.69	0.16	0.28	0.04	42	0.73	0.12	0.26	0.04	35		
	MemPot	0.94	0.81	0.96	0	7	1.00	1.00	1.00	0	1		
IKEA	Optimal-Seq	0.78	0.20	0.36	0.05	12	0.79	0.17	0.34	0.06	14		
	MemPot	1.00	0.98	1.00	0	2	1.00	1.00	1.00	0	2		

Table 6. Comparison of different LLR estimation methods (Sec. 4.3) on MEXTRA_{Cosine}.

Method	EHRAgent						RAP-web					
	AUROC	TPR@1%FPR	TPR@10%FPR	FDT	AUROC	TPR@1%FPR	TPR@10%FPR	FDT				
Count	0.99	0.97	1.00	2	1.00	0.94	1.00	3				
Similarity	0.74	0.65	0.75	4	1.00	0.92	1.00	3				
Global-Sim	1.00	0.98	1.00	1	1.00	0.90	1.00	1				

Table 7. Utility impact of the *MemPot* defense on standard task performance.

Setting	RAP WebShop		Pokémon QA & MCQ		
	Score	Success Rate	Acc	Rouge-L	Sim
w/o pots	67.1	44.6	0.98	0.67	0.75
w/ pots	65.4	43.8	0.98	0.66	0.75

detection time to just 2 rounds. This confirms that proactive distribution modification is essential to break the limits of static detection.

5.5. Utility Impact of *MemPot*

To verify utility preservation, we evaluate *MemPot* on standard tasks on benign user traces. For internal memory dependent tasks, we evaluate Score and Success Rate (defined in RAP (Kagaya et al., 2024)) on WebShop benchmark (Yao et al., 2022). For external memory dependent tasks, we evaluate Accuracy (Acc), Similarity (Sim) and Rouge-L scores on QA and MCQ tasks, with the same setting of IKEA (Wang et al., 2025b). As shown in Tab. 7, *MemPot* has negligible impact on standard agent capabilities, with the Success Rate on the WebShop dropping only marginally from 44.6 to 43.8 and Pokémon QA metrics remain almost

unchanged, confirming that our optimized honeypots are non-disruptive to benign user interactions. We also provide several examples of honeypot documents to show that they are harmless and cause no negative impact, even when retrieved by benign users (Appendix. H).

5.6. Analysis of Different LLR Estimation Methods

We compare three LLR estimation methods (Sec. 4.3) on MEXTRA_{Cosine} (Tab. 6). The Count-based method offers the best trade-off (> 0.99 AUROC, FDT ≈ 2) and is adopted as our default. While Global-similarity achieves the fastest detection at the cost of FPR stability, the Similarity-based method proves suboptimal on complex tasks (e.g., 0.74 AUROC on EHRAgent).

6. Conclusion

We propose *MemPot*, an active defense framework that safeguards agent memory by reshaping retrieval distributions with honeypots to amplify adversarial signals. Overcoming the theoretical limits of passive detection, *MemPot* achieves near-perfect accuracy against advanced threats like IKEA and MEXTRA with zero online latency and preserving agent utility.

Impact Statement

This paper presents work aimed at advancing the security and privacy of Large Language Model (LLM) agents. By mitigating the risks of knowledge extraction in Retrieval-Augmented Generation (RAG) and agentic memory systems, our framework contributes to the protection of proprietary intellectual property and sensitive user data, particularly in high-stakes domains such as healthcare and finance. We believe this work fosters the trustworthy deployment of autonomous agents by ensuring that memory capabilities do not become vulnerabilities. We do not foresee immediate negative societal consequences, as our active defense mechanism is designed to distinguish malicious probing from legitimate usage, minimizing the risk of disrupting normal service.

References

Abbasian, M., Azimi, I., Rahmani, A. M., and Jain, R. C. Conversational health agents: A personalized llm-powered agent framework. *CoRR*, abs/2310.02374, 2023. doi: 10.48550/ARXIV.2310.02374. URL <https://doi.org/10.48550/arXiv.2310.02374>.

Achiam, J., Adler, S., Agarwal, S., Ahmad, L., Akkaya, I., Aleman, F. L., Almeida, D., Altenschmidt, J., Altman, S., Anadkat, S., et al. Gpt-4 technical report. *arXiv preprint arXiv:2303.08774*, 2023.

Agarwal, D., Fabbri, A. R., Risher, B., Laban, P., Joty, S., and Wu, C.-S. Prompt leakage effect and mitigation strategies for multi-turn llm applications. In *Proceedings of the 2024 Conference on Empirical Methods in Natural Language Processing: Industry Track*, pp. 1255–1275, 2024.

Anderson, M., Amit, G., and Goldsteen, A. Is my data in your retrieval database? membership inference attacks against retrieval augmented generation. *arXiv preprint arXiv:2405.20446*, 2024.

asoria. Pokemoninfo dataset, 2024. URL https://huggingface.co/datasets/asoria/pokemon_info.

Cohen, S., Bitton, R., and Nassi, B. Unleashing worms and extracting data: Escalating the outcome of attacks against rag-based inference in scale and severity using jailbreaking. *arXiv preprint arXiv:2409.08045*, 2024.

Cover, T. and Thomas, J. *Elements of Information Theory*. Wiley, 2012. ISBN 9781118585771. URL <https://books.google.com.sg/books?id=VWq5GG6ycxMC>.

Cybenko, G. Approximation by superpositions of a sigmoidal function. *Mathematics of control, signals and systems*, 2(4):303–314, 1989.

Di Maio, C., Cosci, C., Maggini, M., Poggioni, V., and Melacci, S. Pirates of the rag: Adaptively attacking llms to leak knowledge bases. *arXiv preprint arXiv:2412.18295*, 2024.

Ding, H., Li, Y., Wang, J., and Chen, H. Large language model agent in financial trading: A survey, 2024. URL <https://arxiv.org/abs/2408.06361>.

Fan, W., Ding, Y., Ning, L., Wang, S., Li, H., Yin, D., Chua, T.-S., and Li, Q. A survey on rag meeting llms: Towards retrieval-augmented large language models. In *Proceedings of the 30th ACM SIGKDD Conference on Knowledge Discovery and Data Mining*, pp. 6491–6501, 2024.

Grattafiori, A., Dubey, A., Jauhri, A., Pandey, A., Kadian, A., Al-Dahle, A., Letman, A., Mathur, A., Schelten, A., Vaughan, A., et al. The llama 3 herd of models. *arXiv e-prints*, pp. arXiv–2407, 2024.

He, P., Gao, J., and Chen, W. Debertav3: Improving deberta using electra-style pre-training with gradient-disentangled embedding sharing. *arXiv preprint arXiv:2111.09543*, 2021.

Hong, S., Zhuge, M., Chen, J., Zheng, X., Cheng, Y., Wang, J., Zhang, C., Wang, Z., Yau, S. K. S., Lin, Z., Zhou, L., Ran, C., Xiao, L., Wu, C., and Schmidhuber, J. MetaGPT: Meta programming for a multi-agent collaborative framework. In *The Twelfth International Conference on Learning Representations*, 2024. URL <https://openreview.net/forum?id=VtmBAGCN7o>.

Hu, Y., Liu, S., Yue, Y., Zhang, G., Liu, B., Zhu, F., Lin, J., Guo, H., Dou, S., Xi, Z., et al. Memory in the age of ai agents. *arXiv preprint arXiv:2512.13564*, 2025.

Jiang, C., Pan, X., Hong, G., Bao, C., and Yang, M. Ragthief: Scalable extraction of private data from retrieval-augmented generation applications with agent-based attacks. *arXiv preprint arXiv:2411.14110*, 2024.

Kagaya, T., Yuan, T. J., Lou, Y., Karlekar, J., Pranata, S., Kinose, A., Oguri, K., Wick, F., and You, Y. RAP: retrieval-augmented planning with contextual memory for multimodal LLM agents. *CoRR*, abs/2402.03610, 2024. doi: 10.48550/ARXIV.2402.03610. URL <https://doi.org/10.48550/arXiv.2402.03610>.

Kulkarni, M., Tangarajan, P., Kim, K., and Trivedi, A. Reinforcement learning for optimizing RAG for domain chatbots. *CoRR*, abs/2401.06800, 2024. doi: 10.48550/ARXIV.2401.06800. URL <https://doi.org/10.48550/arXiv.2401.06800>.

lavita AI. lavita/chatdoctor-healthcaremagic-100k · datasets at hugging face. URL <https://huggingface.co/datasets/lavita/ChatDoctor-HealthCareMagic-100k>.

Lewis, P. S. H., Perez, E., Piktus, A., Petroni, F., Karpukhin, V., Goyal, N., Kütterer, H., Lewis, M., Yih, W., Rocktäschel, T., Riedel, S., and Kiela, D. Retrieval-augmented generation for knowledge-intensive NLP tasks. In Larochelle, H., Ranzato, M., Hadsell, R., Balcan, M., and Lin, H. (eds.), *Advances in Neural Information Processing Systems 33: Annual Conference on Neural Information Processing Systems 2020, NeurIPS 2020, December 6-12, 2020, virtual*, 2020. URL <https://proceedings.neurips.cc/paper/2020/hash/6b493230205f780e1bc26945df7481e5-Abstract.html>.

Li, Y., Li, Z., Zhang, K., Dan, R., and Zhang, Y. Chatdoctor: A medical chat model fine-tuned on llama model using medical domain knowledge. *CoRR*, abs/2303.14070, 2023. doi: 10.48550/ARXIV.2303.14070. URL <https://doi.org/10.48550/arXiv.2303.14070>.

Liu, A., Feng, B., Xue, B., Wang, B., Wu, B., Lu, C., Zhao, C., Deng, C., Zhang, C., Ruan, C., et al. Deepseek-v3 technical report. *arXiv preprint arXiv:2412.19437*, 2024.

Mao, J., Ye, J., Qian, Y., Pavone, M., and Wang, Y. A language agent for autonomous driving. *CoRR*, abs/2311.10813, 2023. doi: 10.48550/ARXIV.2311.10813. URL <https://doi.org/10.48550/arXiv.2311.10813>.

Noma Security. ForcedLeak: Agent Risks Exposed in Salesforce Agentforce. <https://noma.security/blog/forcedleak-agent-risks-exposed-in-salesforce-agentforce>, 2024. Accessed: Jan 6, 2026.

OpenAI. GPT-4 technical report. *CoRR*, abs/2303.08774, 2023. doi: 10.48550/arXiv.2303.08774. URL <https://doi.org/10.48550/arXiv.2303.08774>.

Qi, Z., Zhang, H., Xing, E. P., Kakade, S. M., and Lakkaraju, H. Follow my instruction and spill the beans: Scalable data extraction from retrieval-augmented generation systems. In *International Conference on Learning Representations (ICLR)*, 2025.

Salesforce. Agentforce: The AI Agent Platform. <https://www.salesforce.com/eu/agentforce/>, 2024. Accessed: Jan 6, 2026.

Sason, I. and Verdú, S. Bounds among f-divergences. *submitted to the IEEE Trans. on Information Theory*, 2015.

Shi, W., Xu, R., Zhuang, Y., Yu, Y., Zhang, J., Wu, H., Zhu, Y., Ho, J. C., Yang, C., and Wang, M. D. Ehrlagent: Code empowers large language models for few-shot complex tabular reasoning on electronic health records. In Al-Onaizan, Y., Bansal, M., and Chen, Y. (eds.), *Proceedings of the 2024 Conference on Empirical Methods in Natural Language Processing, EMNLP 2024, Miami, FL, USA, November 12-16, 2024*, pp. 22315–22339. Association for Computational Linguistics, 2024. URL <https://aclanthology.org/2024.emnlp-main.1245>.

Song, K., Tan, X., Qin, T., Lu, J., and Liu, T.-Y. Mpnet: Masked and permuted pre-training for language understanding. *Advances in neural information processing systems*, 33:16857–16867, 2020.

Wald, A. Sequential tests of statistical hypotheses. In *Breakthroughs in statistics: Foundations and basic theory*, pp. 256–298. Springer, 1992.

Wald, A. and Wolfowitz, J. Optimum character of the sequential probability ratio test. *The Annals of Mathematical Statistics*, pp. 326–339, 1948.

Wang, B., He, W., Zeng, S., Xiang, Z., Xing, Y., Tang, J., and He, P. Unveiling privacy risks in llm agent memory. In *Proceedings of the 63rd Annual Meeting of the Association for Computational Linguistics (Volume 1: Long Papers)*, pp. 25241–25260, 2025a.

Wang, L., Ma, C., Feng, X., Zhang, Z., Yang, H., Zhang, J., Chen, Z., Tang, J., Chen, X., Lin, Y., et al. A survey on large language model based autonomous agents. *Frontiers of Computer Science*, 18(6):186345, 2024.

Wang, Y., Qu, W., Zhai, S., Jiang, Y., Liu, Z., Liu, Y., Dong, Y., and Zhang, J. Silent leaks: Implicit knowledge extraction attack on rag systems through benign queries, 2025b. URL <https://arxiv.org/abs/2505.15420>.

Xi, Z., Chen, W., Guo, X., He, W., Ding, Y., Hong, B., Zhang, M., Wang, J., Jin, S., Zhou, E., et al. The rise and potential of large language model based agents: A survey. *arXiv preprint arXiv:2309.07864*, 2023.

Yao, H., Shi, H., Chen, Y., Jiang, Y., Wang, C., Qin, Z., Ren, K., and Chen, C. Controlnet: A firewall for rag-based llm system. *arXiv preprint arXiv:2504.09593*, 2025.

Yao, S., Chen, H., Yang, J., and Narasimhan, K. Webshop: Towards scalable real-world web interaction with grounded language agents. In Koyejo, S., Mohamed, S., Agarwal, A., Belgrave, D., Cho, K., and Oh, A. (eds.), *Advances in Neural Information Processing Systems 35: Annual Conference on Neural Information Processing Systems 2022, NeurIPS*

2022, *New Orleans, LA, USA, November 28 - December 9, 2022*. URL http://papers.nips.cc/paper_files/paper/2022/hash/82ad13ec01f9fe44c01cb91814fd7b8c-Abstract-Conference.html.

Yao, S., Zhao, J., Yu, D., Du, N., Shafran, I., Narasimhan, K. R., and Cao, Y. React: Synergizing reasoning and acting in language models. In *The Eleventh International Conference on Learning Representations, ICLR 2023, Kigali, Rwanda, May 1-5, 2023*. OpenReview.net, 2023. URL https://openreview.net/forum?id=WE_vluYUL-X.

Zeng, S., Zhang, J., He, P., Liu, Y., Xing, Y., Xu, H., Ren, J., Chang, Y., Wang, S., Yin, D., and Tang, J. The good and the bad: Exploring privacy issues in retrieval-augmented generation (RAG). In *Findings of the Association for Computational Linguistics: ACL 2024*, pp. 4505–4524, 2024a.

Zeng, S., Zhang, J., He, P., Ren, J., Zheng, T., Lu, H., Xu, H., Liu, H., Xing, Y., and Tang, J. Mitigating the privacy issues in retrieval-augmented generation (RAG) via pure synthetic data. *arXiv preprint arXiv:2406.14773*, 2025.

Zeng, Y., Wu, Y., Zhang, X., Wang, H., and Wu, Q. Autodefense: Multi-agent llm defense against jailbreak attacks. *arXiv preprint arXiv:2403.04783*, 2024b.

Zhang, C., Zhang, T., and Shmatikov, V. Adversarial decoding: Generating readable documents for adversarial objectives, 2025. URL <https://arxiv.org/abs/2410.02163>.

Zhang, Y., Ding, L., Zhang, L., and Tao, D. Intention analysis makes llms a good jailbreak defender. *arXiv preprint arXiv:2401.06561*, 2024a.

Zhang, Z., Bo, X., Ma, C., Li, R., Chen, X., Dai, Q., Zhu, J., Dong, Z., and Wen, J. A survey on the memory mechanism of large language model based agents. *CoRR*, abs/2404.13501, 2024b. doi: 10.48550/ARXIV.2404.13501. URL <https://doi.org/10.48550/arXiv.2404.13501>.

Zhao, W. X., Zhou, K., Li, J., Tang, T., Wang, X., Hou, Y., Min, Y., Zhang, B., Zhang, J., Dong, Z., et al. A survey of large language models. *arXiv preprint arXiv:2303.18223*, 2023.

A. Details of Honeypot optimization

Attacker Proxy. In practical settings, the detailed algorithms and objectives of attackers are often not accessible, making it difficult to obtain an exact attack query distribution \mathcal{Q}_1 . To address this, we construct an *attacker proxy* that learns to reproduce the attacker’s behavior at the sentence embedding level. The proxy is realized as a neural network A_ω that, given the historical interaction trajectory $\{o_{1:t-1}\}$ —including previous query embeddings, retrieved document indices, and similarity scores—iteratively outputs the embedding of the next query $\hat{e}_t = A_\omega(o_{1:t-1})$. Instead of reconstructing the attacker’s internal algorithm, the goal of A_ω is to mimic the observable embedding-level dynamics of the attacker. The training objective minimizes the discrepancy between the generated embeddings and the observed ones using cosine similarity regression, ensuring that the proxy reproduces similar retrieval rankings under the same retriever. This design allows the honeypot system to train defensive strategies without explicit access to the attacker’s model parameters.

User Proxy. For normal user modeling, we face a similar challenge: the real-world user query distribution is difficult to collect and often highly diverse. To approximate it, we leverage the large language model’s (LLM) human-simulator capability to synthesize realistic user behaviors. Specifically, we utilize a human-simulation pipeline that prompts the LLM with interaction intents and retrieval contexts, generating natural multi-turn query sequences that resemble genuine information-seeking behavior. These synthetic user queries are then encoded into embeddings to approximate the benign query distribution \mathcal{Q}_0 .

B. Details of Experiment Setups

B.1. Setups

Datasets and Evaluation Setting. We evaluate *MemPot* across four diverse benchmarks covering both external memory retrieval and internal memory interaction scenarios: For external memory, we utilize the HealthMagicCare (20k rows) ([lavita AI](#)) and Pokémon (9.46k rows) ([asoria](#), 2024) datasets, representing privacy-intensive healthcare inquiries and entity-heavy gaming knowledge, respectively. We default retrieve 4 documents each turn in experiments. For internal memory, following the setting in MEXTRA ([Wang et al., 2025a](#)), we use the generated internal memory logs for EHRAgent ([Shi et al., 2024](#)) and RAP on WebShop ([Yao et al., 2022](#); [Kagaya et al., 2024](#)). The standard setting contains 300 interaction records. We follow the same retrieval number setting (top-4 records for EHRAgent and top-3 for RAP WebShop) in origin paper ([Shi et al., 2024](#); [Kagaya et al., 2024](#)). For scalability analysis (Appendix. C.1), we extend this by appending an additional 200 records. We employ DeepSeek-v3.2 (685B) as the backbone model of both agents and all-mpnet-base-v2 as the retrieval embedding model. We use mDeBERTa-v3-base ([He et al., 2021](#)) as NLI model. For each dataset/agent, we use the same honeypot set against different attacks. We inject honeypots at a ratio of 2% for external memory datasets and 4% for internal memory datasets by default (We evaluate the impact of honeypots ratio in Appendix. C.2). For the SPRT detector, we utilize the Pot-NonPot Counts Ratio (Eq. 17) as the default method for LLR estimation with both type-I/II error budgets α, β set to 0.1. All experiments are conducted on a single NVIDIA RTX 5090 GPU.

Training Set Configuration. We train a transformer-based attacker proxy using 256 samples for each attack type. To robustly capture the exploratory nature of extraction attacks, we augment the training data using a similarity top-k random walk, which simulates an attacker’s trajectory by iteratively sampling the next query from the semantic neighbors of the current retrieval. The honeypots are trained by interacting with this proxy, while simultaneously optimizing contrastive loss against 500 LLM-generated benign human queries for each target dataset. To support honeypots’ training on large-scale knowledge bases, we first apply balanced k-means clustering to partition the document corpus into equal-sized sets. The document embeddings within each set are fed into a shared network to generate a corresponding honeypot embedding, significantly reducing the computational burden of generation.

Attacks and Defense Baselines. We consider the following attacks: For external memory, we evaluate RAG-targeted adaptive attacks including RAG-Thief ([Jiang et al., 2024](#)), DGEA ([Cohen et al., 2024](#)), and IKEA ([Wang et al., 2025b](#)). For internal memory, we evaluate agent-targeted MEXTRA ([Wang et al., 2025a](#)). Additionally, we adapt IKEA for internal memory extraction to assess robustness against adaptive attacks. We broadly consider existing defense methods, including ControlNet ([Yao et al., 2025](#)) and Agent Detector ([Zhang et al., 2024a](#); [Zeng et al., 2024b](#); [Agarwal et al., 2024](#)). Specifically, we use 100 benign anchor queries for ControlNet initiation and DeepSeek-v3.2 (685B) as the Agent Detector backbone (see Appendix B.2). We additionally design a transformer-based theoretical optimal sequential detector (Optimal-Seq) for further comparison and validation of Thm. 2.

Table 8. Performance evaluation of stacked MemPot and end-to-end trained MemPot on EHRAgent and Web-Shopping RAP agent.

Attack	Defense	EHRAgent					RAP-web				
		AUROC	TP@1%FP	TP@10%FP	Delay	FDT	AUROC	TP@1%FP	TP@10%FP	Delay	FDT
MEXTRA _{Cosine}	Optimal-Seq	0.70	0.16	0.27	0.03	22	0.68	0.06	0.22	0.04	38
	MemPot-E2E	0.99	0.67	0.74	0	2	0.98	1.00	1.00	0	1
	MemPot-Stack	0.98	0.65	0.75	0	3	0.99	1.00	1.00	0	1
MEXTRA _{Edit}	Optimal-Seq	0.71	0.14	0.32	0.04	33	0.75	0.20	0.36	0.04	27
	MemPot-E2E	0.98	0.56	0.74	0	4	1.00	1.00	1.00	0	1
	MemPot-Stack	0.97	0.58	0.72	0	9	1.00	1.00	1.00	0	1
MEXTRA _{General}	Optimal-Seq	0.69	0.16	0.28	0.04	42	0.73	0.12	0.26	0.04	35
	MemPot-E2E	0.94	0.81	0.85	0	7	1.00	1.00	1.00	0	1
	MemPot-Stack	0.98	0.82	0.88	0	5	1.00	1.00	1.00	0	1

B.2. Agent Detector Setting

Referring to mitigation suggestions in (Zeng et al., 2024a; Jiang et al., 2024; Anderson et al., 2024; Zhang et al., 2024a; Zeng et al., 2024b), We apply the agent detector with hybrid paradigms, including intention detection, keyword detection and defensive instruction. Specifically, we use DeepSeek-v3.2 (685B) as the agent detector backbone. The response generation process integrated with the detector is shown as follows: For an input query q , defense first occurs through intent detection (Zhang et al., 2024a) and keyword filtering (Zeng et al., 2024a):

$$q_{\text{defended}} = \begin{cases} \emptyset, & D_{\text{intent}}(q) \vee D_{\text{keyword}}(q) = 1, \\ q, & \text{otherwise} \end{cases}, \quad (20)$$

where \emptyset enforces an “unanswerable” response, $D_{\text{intent}}(\cdot)$ and $D_{\text{keyword}}(\cdot)$ are detection functions which return True when detecting malicious extraction intention or words. When $q_{\text{defended}} \neq \emptyset$, generation combines the retrieval context \mathcal{D}_q^K is:

$$y = \text{LLM}(\text{Concat}(\mathcal{D}_q^K) \oplus q_{\text{defended}} \oplus p_{\text{defense}}), \quad (21)$$

where defensive prompt p_{defense} (Agarwal et al., 2024) constrains output relevance by prompting LLM only answer with related part of retrievals, and enforces LLM not responding to malicious instruction with provided examples.

C. Additional Experiments

C.1. Scalability of MemPot under Memory Updates

To address the dynamic nature of agent systems where memory is updated in real-time, we evaluate the scalability of *MemPot* using a batch-based update strategy. Leveraging the localized nature of retrieval, we hypothesize that honeypots can be optimized independently for different memory batches and directly merged into a unified defense set.

Setup. We simulate a memory update scenario by appending 200 new interaction records (sourced from the MEXTRA dataset (Wang et al., 2025a)) to the standard 300-record internal memory, resulting in a total of 500 records. We compare two implementation strategies: (1) **MemPot-E2E**: The computationally expensive upper bound, where honeypots are re-optimized globally on the complete 500-record dataset from scratch. (2) **MemPot-Stack**: The scalable approach, where we retain the honeypots for the initial 300 records and simply append a new set of honeypots optimized specifically for the 200 update records. To ensure a fair comparison, we maintain the honeypot ratio at 4% for both strategies.

Results. As shown in Tab. 8, *MemPot-Stack* achieves detection performance nearly identical to the holistic *MemPot-e2e* across all attack vectors. Notably, in challenging scenarios like MEXTRA-General on EHRAgent, the stacked approach maintains superior robustness (0.98 AUROC) compared to the end-to-end baseline (0.94 AUROC). These results confirm that *MemPot* supports efficient, modular updates: as the agent’s memory grows, new honeypots can be seamlessly integrated without the need for global retraining, ensuring continuous protection with minimal computational overhead.

Table 9. Ablation study on the number of pots (honeypots) and their impact on detection performance on MEXTRA_{cosine} in RAP WebShop.

Ratio	AUROC	TP@1%FP	TP@10%FP	FDT
0.6%	1.00	0.77	1.00	7
1.0%	1.00	0.79	1.00	4
2.0%	1.00	0.90	1.00	2
4.0%	1.00	0.94	1.00	2

C.2. Impact of Honeypots Number

We investigate the trade-off between ratio of injected honeypots and detection robustness. Tab. 9 reports the detection performance on the RAP WebShop with 300 memory records as the honeypots ratio increases from 0.6% to 4%. While the AUROC remains saturated at 1.00 even with minimal injection, increasing the honeypot count significantly enhances detection speed and sensitivity at strict thresholds. Specifically, increasing pots from 0.6% to 4% improves the TP@1%FP from 0.77 to 0.94 and reduces the First Detection Time (FDT) from 7 rounds to just 2 rounds. This trend validates that a denser honeypot distribution amplifies the adversarial signal, allowing for faster interception of attacks, though a small budget (e.g., 2%) already yields near-optimal performance.

D. Theoretical Preliminary

Definition 1 (Fixed parametric partition). Let $T_\phi : \mathcal{O} \rightarrow \mathcal{Y}$ be a fixed-form parametric partition (its *form* does not change during training; only parameters ϕ change). Define the push-forwards

$$P_{1,\theta,\phi} = T_{\phi\#} f_{1,\theta}, \quad P_{0,\theta,\phi} = T_{\phi\#} f_{0,\theta},$$

and the divergence $\Phi_T(\theta, \phi) = \text{KL}(P_{1,\theta,\phi} \| P_{0,\theta,\phi})$.

Lemma 1 (Data Processing Inequality (DPI)). *For any measurable T_ϕ ,*

$$\text{KL}(f_{1,\theta} \| f_{0,\theta}) \geq \text{KL}(T_{\phi\#} f_{1,\theta} \| T_{\phi\#} f_{0,\theta}) = \Phi_T(\theta, \phi).$$

Likewise, $\text{KL}(f_{0,\theta} \| f_{1,\theta}) \geq \text{KL}(P_{0,\theta,\phi} \| P_{1,\theta,\phi})$.

Proof. Classic DPI; see *Step 1* of Lemma 3's proof. □

Lemma 2 (Conditional expectation over finite partition). *Let (Ω, \mathcal{F}, g) be a probability space, let $\mathcal{P} = \{A_1, \dots, A_m\}$ be a finite measurable partition of Ω , and write $\sigma(\mathcal{P})$ for the σ -algebra it generates. For any $X \in L^1(g)$, define*

$$Y(x) := \sum_{i=1}^m \mathbf{1}_{A_i}(x) \begin{cases} \frac{1}{g(A_i)} \int_{A_i} X dg, & g(A_i) > 0, \\ 0, & g(A_i) = 0. \end{cases}$$

Then:

1. *Y is $\sigma(\mathcal{P})$ -measurable and, for every $B \in \sigma(\mathcal{P})$, $\int_B Y dg = \int_B X dg$. Hence $Y = \mathbb{E}_g[X | \sigma(\mathcal{P})]$ almost surely.*
2. *In particular, writing $\mathbb{E}_g[X | \mathcal{P}]$ as shorthand for $\mathbb{E}_g[X | \sigma(\mathcal{P})]$,*

$$\int \mathbb{E}_g[X | \mathcal{P}] dg = \int X dg. \tag{22}$$

Proof. (1) By construction, Y is constant on each atom A_i , thus $\sigma(\mathcal{P})$ -measurable. If $B = \bigcup_{i \in I} A_i \in \sigma(\mathcal{P})$, then

$$\begin{aligned} \int_B Y dg &= \sum_{i \in I} \frac{1}{g(A_i)} \left(\int_{A_i} X dg \right) g(A_i) \\ &= \sum_{i \in I} \int_{A_i} X dg = \int_B X dg, \end{aligned}$$

which is precisely the defining property of the conditional expectation $\mathbb{E}_g[X \mid \sigma(\mathcal{P})]$. Uniqueness up to g -null sets yields $Y = \mathbb{E}_g[X \mid \sigma(\mathcal{P})]$ a.s.

(2) Take $B = \Omega$ in the identity of part (1) to obtain (22). \square

Lemma 3 (Partition supremum). *For any pair of laws f, g on \mathcal{O} ,*

$$\text{KL}(f\|g) = \sup_T \text{KL}(T\#f\|T\#g),$$

where the supremum is over all finite measurable partitions (equivalently, finite-range measurable maps T); moreover, for any $\delta > 0$ there exists a finite partition T_δ such that

$$\text{KL}(f\|g) \leq \text{KL}(T_\delta\#f\|T_\delta\#g) + \delta.$$

Proof. If $f \ll g$, there exists $A \in \mathcal{F}$ with $g(A) = 0$ and $f(A) > 0$; for the two-atom partition $\{A, A^c\}$ one has $\text{KL}(T\#f\|T\#g) = +\infty = \text{KL}(f\|g)$, and the statement is trivial. Hence assume $f \ll g$. Let $L := \frac{df}{dg}$ and $\ell := \log L$, which are well-defined with Radon-Nikodym theorem. Then $\text{KL}(f\|g) = \int L \log L dg = \int \ell df \in [0, \infty]$.

Step 1 (DPI Inequality).

Let $\mathcal{P} = \{A_i\}_{i=1}^m$ be a finite partition and let T be its index map. Write $p_i = f(A_i) = \int_{A_i} L dg$ and $q_i = g(A_i)$ (with the convention $0 \log 0 := 0$). Then

$$\begin{aligned} \text{KL}(T\#f\|T\#g) &= \sum_{i=1}^m p_i \log \frac{p_i}{q_i} \\ &= \sum_{i=1}^m \left(\int_{A_i} L dg \right) \log \frac{\int_{A_i} L dg}{g(A_i)} \\ &= \int \mathbb{E}_g[L \mid \mathcal{P}] \log \mathbb{E}_g[L \mid \mathcal{P}] dg, \end{aligned}$$

where $\mathbb{E}_g[\cdot \mid \mathcal{P}]$ is conditional expectation under g onto the σ -algebra generated by \mathcal{P} . Since $\varphi(u) := u \log u$ is convex on $(0, \infty)$, Jensen yields $\varphi(\mathbb{E}_g[L \mid \mathcal{P}]) \leq \mathbb{E}_g[\varphi(L) \mid \mathcal{P}]$, and with Lemma 2 integrating gives

$$\begin{aligned} \text{KL}(T\#f\|T\#g) &= \int \varphi(\mathbb{E}_g[L \mid \mathcal{P}]) dg \\ &\leq \int \mathbb{E}_g[\varphi(L) \mid \mathcal{P}] dg \\ &= \int \varphi(L) dg = \text{KL}(f\|g). \end{aligned}$$

Then taking the supremum over all finite \mathcal{P} shows $\sup_T \text{KL}(T\#f\|T\#g) \leq \text{KL}(f\|g)$.

Step 2 (Limitation of divergence gap with a finite partition).

Fix $\delta > 0$ and assume $\text{KL}(f\|g) < \infty$. We construct a finite partition \mathcal{P}_δ for which $\text{KL}(f\|g) - \text{KL}(T_\delta\#f\|T_\delta\#g) \leq \delta$.

(2.a) *Tail control.*

Choose $M \geq 1$ so large that the “upper tail” contribution satisfies

$$\int_{\{L \geq e^M\}} L \log L dg \leq \delta/3,$$

and additionally $2Me^{-M} \leq \delta/3$ (possible since $Me^{-M} \rightarrow 0$ as $M \rightarrow \infty$). Define three regions

$$A_- := \{L < e^{-M}\}, B := \{e^{-M} \leq L < e^M\}, A_+ := \{L \geq e^M\}.$$

(2.b) *Middle quantization.*

Pick a mesh size $\eta \in (0, 1)$ to be specified (below we take $\eta := \delta/3$). Partition the middle region B into finitely many level sets of L : for $k = 0, 1, \dots, K-1$ with $K := \lceil 2M/\eta \rceil$, set

$$B_k := \{x \in \mathcal{O} : e^{-M+k\eta} \leq L(x) < e^{-M+(k+1)\eta}\}.$$

Then on each B_k we have $\log L \in [a_k, a_k + \eta]$ with $a_k := -M + k\eta$, and also

$$\begin{aligned} \log \mathbb{E}_g[L | B_k] &= \log \frac{\int_{B_k} L dg}{g(B_k)} \in [a_k, a_k + \eta] \\ &\Rightarrow |\log L - \log \mathbb{E}_g[L | B_k]| \leq \eta \text{ on } B_k. \end{aligned}$$

(2.c) *The finite partition.*

Let $\mathcal{P}_\delta := \{A_-, B_0, \dots, B_{K-1}, A_+\}$ and let T_δ be its index map. Using the identity from Step 1 and writing the gap as an $L dg$ -integral, we have

$$\text{KL}(f\|g) - \text{KL}(T_\delta f\|T_\delta g) = \sum_{C \in \mathcal{P}_\delta} \int_C L \left(\log L - \log \mathbb{E}_g[L | C] \right) dg =: \Delta_- + \Delta_B + \Delta_+.$$

(2.d) *Bounding the middle gap.*

On each B_k , the pointwise bound $|\log L - \log \mathbb{E}_g[L | B_k]| \leq \eta$ yields

$$\Delta_B = \sum_{k=0}^{K-1} \int_{B_k} L \left(\log L - \log \mathbb{E}_g[L | B_k] \right) dg \leq \eta \sum_{k=0}^{K-1} \int_{B_k} L dg = \eta f(B) \leq \eta.$$

(2.e) *Bounding the lower-tail gap.*

On A_- one has $L \leq e^{-M}$. Using $|\log L - \log \mathbb{E}_g[L | A_-]| \leq |\log L| + |\log \mathbb{E}_g[L | A_-]|$ and $\mathbb{E}_g[L | A_-] \leq e^{-M} \Rightarrow |\log \mathbb{E}_g[L | A_-]| \leq -M$, we obtain

$$\Delta_- \leq \int_{A_-} L |\log L| dg + M \int_{A_-} L dg \leq M e^{-M} + M e^{-M} = 2M e^{-M} \leq \delta/3,$$

by the choice of M .

(2.f) *Bounding the upper-tail gap.* On A_+ one has $\mathbb{E}_g[L | A_+] \geq e^M$, so $\log L - \log \mathbb{E}_g[L | A_+] \leq \log L - M$. Hence

$$0 \leq \Delta_+ = \int_{A_+} L \left(\log L - \log \mathbb{E}_g[L | A_+] \right) dg \leq \int_{A_+} L (\log L - M) dg \leq \int_{A_+} L \log L dg \leq \delta/3,$$

by the choice of M .

(2.g) *Total control.*

Set $\eta := \delta/3$. Collecting the bounds from (2.d)–(2.f) gives

$$\text{KL}(f\|g) - \text{KL}(T_\delta f\|T_\delta g) \leq \delta/3 + \delta/3 + \delta/3 = \delta.$$

Step 3 (Taking the supremum).

By Step 1, $\text{KL}(T_\# f\|T_\# g) \leq \text{KL}(f\|g)$ for every finite partition. By Step 2, for each $\delta > 0$ there exists a finite partition T_δ such that $\text{KL}(f\|g) \leq \text{KL}(T_\delta f\|T_\delta g) + \delta$. Therefore $\sup_T \text{KL}(T_\# f\|T_\# g) \geq \text{KL}(f\|g) - \delta$ for all $\delta > 0$, hence $\sup_T \text{KL}(T_\# f\|T_\# g) = \text{KL}(f\|g)$. \square

Lemma 4 (Cross-entropy dominates the Bayes risk). *Let $J \in \{1, \dots, K\}$ and $\mathbf{Y} = (Y_1, \dots, Y_K)$ be generated as in the 1-positive $(K-1)$ -negative scheme, and let $\pi^*(j \mid \mathbf{Y})$ denote the true posterior of J given \mathbf{Y} . For any measurable score $h : \mathcal{Y} \rightarrow \mathbb{R}$, define the model posterior $\pi_h(j \mid \mathbf{Y}) := \frac{e^{h(Y_j)}}{\sum_{i=1}^K e^{h(Y_i)}}$ and the K -sample InfoNCE loss*

$$\mathcal{L}_{\text{NCE},K}(h) := \mathbb{E}[-\log \pi_h(J \mid \mathbf{Y})].$$

Then

$$\mathcal{L}_{\text{NCE},K}(h) \geq \mathbb{E}_{\mathbf{Y}}[H(\pi^*(\cdot \mid \mathbf{Y}))] \iff -\mathcal{L}_{\text{NCE},K}(h) \leq -\mathcal{L}^*, \quad (23)$$

where $H(p) := -\sum_j p(j) \log p(j)$ and $\mathcal{L}^* := \mathbb{E}_{\mathbf{Y}}[H(\pi^*(\cdot \mid \mathbf{Y}))]$ is the Bayes risk when taking logarithmic loss. Equality holds iff $\pi_h(\cdot \mid \mathbf{Y}) = \pi^*(\cdot \mid \mathbf{Y})$ a.s.

Proof. For fixed \mathbf{Y} , by the standard decomposition $H(p, q) = H(p) + \text{KL}(p\|q)$, the cross-entropy between π^* and π_h is

$$H(\pi^*, \pi_h) = \mathbb{E}_{J \sim \pi^*(\cdot \mid \mathbf{Y})}[-\log \pi_h(J \mid \mathbf{Y})] = H(\pi^*) + \text{KL}(\pi^*(\cdot \mid \mathbf{Y}) \parallel \pi_h(\cdot \mid \mathbf{Y})).$$

Since $\text{KL}(\cdot \parallel \cdot) \geq 0$ (Gibbs' inequality (Cover & Thomas, 2012)), we have $H(\pi^*, \pi_h) \geq H(\pi^*)$ with equality iff $\pi_h = \pi^*$. Taking expectation over \mathbf{Y} gives

$$\mathcal{L}_{\text{NCE},K}(h) = \mathbb{E}_{\mathbf{Y}}[H(\pi^*, \pi_h)] \geq \mathbb{E}_{\mathbf{Y}}[H(\pi^*)] = \mathcal{L}^*,$$

which is (23). \square

Lemma 5 (Conditional product density under a uniform index). *Let P, Q be probability laws on $(\mathcal{Y}, \mathcal{G})$ with $P \ll Q$, and set $r := \frac{dP}{dQ}$. Fix $K \geq 2$. Draw $J \sim \text{Unif}\{1, \dots, K\}$ and, given $J = j$, sample $\mathbf{Y} = (Y_1, \dots, Y_K)$ with independent coordinates $Y_j \sim P$ and $Y_i \sim Q$ for $i \neq j$. Then:*

1. *For each j , the conditional law $\mathbb{P}(\mathbf{Y} \mid J = j)$ is absolutely continuous w.r.t. $Q^{\otimes K}$ with Radon–Nikodym derivative*

$$\frac{d\mathbb{P}(\mathbf{Y} \mid J = j)}{dQ^{\otimes K}}(\mathbf{y}) = r(y_j) \quad (Q^{\otimes K}\text{-a.e.}).$$

2. *The marginal law of \mathbf{Y} satisfies*

$$\frac{d\mathbb{P}_{\mathbf{Y}}}{dQ^{\otimes K}}(\mathbf{y}) = \frac{1}{K} \sum_{i=1}^K r(y_i) \quad (Q^{\otimes K}\text{-a.e.}).$$

Proof. We use the test-function characterization of Radon–Nikodym derivatives.

(1) *Conditional law.* Fix $j \in \{1, \dots, K\}$ and any bounded measurable $\varphi : \mathcal{Y}^K \rightarrow \mathbb{R}$. By the construction of \mathbf{Y} given $J = j$ and independence of coordinates,

$$\int \varphi(\mathbf{y}) d\mathbb{P}(\mathbf{Y} \mid J = j) = \int \varphi(\mathbf{y}) d(Q^{\otimes(j-1)} \otimes P \otimes Q^{\otimes(K-j)})(\mathbf{y}).$$

Since $P \ll Q$ with density $r = \frac{dP}{dQ}$ and $Q \ll Q$ with density 1, we have for $Q^{\otimes K}$ almost everywhere on \mathbf{y} ,

$$\frac{d(Q^{\otimes(j-1)} \otimes P \otimes Q^{\otimes(K-j)})}{d(Q^{\otimes K})}(\mathbf{y}) = r(y_j) \cdot \prod_{i \neq j} 1 = r(y_j),$$

and therefore

$$\int \varphi(\mathbf{y}) d\mathbb{P}(\mathbf{Y} \mid J = j) = \int \varphi(\mathbf{y}) r(y_j) d(Q^{\otimes K})(\mathbf{y}).$$

By uniqueness in the Radon–Nikodym theorem, this identifies $\frac{d\mathbb{P}(\mathbf{Y} \mid J = j)}{dQ^{\otimes K}} = r(y_j)$ almost everywhere.

(2) *Marginal law.* Averaging over the uniform J ,

$$\int \varphi(\mathbf{y}) d\mathbb{P}_{\mathbf{Y}} = \sum_{j=1}^K \mathbf{1}(J=j) \int \varphi(\mathbf{y}) d\mathbb{P}(\mathbf{Y} \mid J=j) = \frac{1}{K} \sum_{j=1}^K \int \varphi(\mathbf{y}) r(y_j) d(Q^{\otimes K})(\mathbf{y}).$$

Hence, again by Radon–Nikodym uniqueness, $\frac{d\mathbb{P}_{\mathbf{Y}}}{dQ^{\otimes K}}(\mathbf{y}) = \frac{1}{K} \sum_{j=1}^K r(y_j) Q^{\otimes K}$. \square

Lemma 6 (ASN Approximation for SPRT with Markov Observations). *Consider the SPRT with boundaries $A < 0 < B$ and error budgets (α, β) . Let the observation sequence $\{O_t\}_{t=1}^{\infty}$ be a stationary and ergodic Markov chain under each hypothesis, with transition densities $f_{1,\theta}$ and $f_{0,\theta}$. Let $\ell_{\theta}(O_t|O_{t-1}) = \log \frac{f_{1,\theta}(O_t|O_{t-1})}{f_{0,\theta}(O_t|O_{t-1})}$ be the per-step log-likelihood ratio. Define the drift rates under H_1 and H_0 respectively as*

$$\mu_1(\theta) = \mathbb{E}_{1,\theta}[\ell_{\theta}(O_t|O_{t-1})], \quad \mu_0(\theta) = \mathbb{E}_{0,\theta}[\ell_{\theta}(O_t|O_{t-1})].$$

If the overshoot at stopping is negligible, then the expected stopping times (ASN) are approximately

$$\mathbb{E}_1[N] \approx \frac{|\log B|}{\mu_1(\theta)}, \quad \mathbb{E}_0[N] \approx \frac{|\log A|}{\mu_0(\theta)}. \quad (24)$$

Proof. We give a detailed proof under the assumption of stationary, ergodic Markov observations.

Let $\{O_t\}_{t \geq 0}$ be a Markov chain on a state space \mathcal{O} . Under hypothesis H_i ($i = 0, 1$), the chain has transition density $f_{i,\theta}(\cdot|O_{t-1})$ and a unique stationary distribution π_i . We assume the chain starts from its stationary distribution (or an arbitrary initial distribution; by ergodicity the long-run behavior is the same). The per-step log-likelihood ratio is

$$Z_t \equiv \ell_{\theta}(O_t|O_{t-1}) = \log \frac{f_{1,\theta}(O_t|O_{t-1})}{f_{0,\theta}(O_t|O_{t-1})},$$

and the cumulative sum is $S_n = \sum_{t=1}^n Z_t$. The stopping time is

$$N = \inf\{n \geq 1 : S_n \geq \log B \text{ or } S_n \leq \log A\},$$

where the boundaries satisfy $A = \frac{\beta}{1-\alpha}$ and $B = \frac{1-\beta}{\alpha}$ for given error probabilities α, β (Wald's approximations).

By stationarity,

$$\mu_1(\theta) = \mathbb{E}_{1,\theta}[Z_t] = \iint \pi_1(dx) f_{1,\theta}(dy|x) \log \frac{f_{1,\theta}(dy|x)}{f_{0,\theta}(dy|x)} = \text{KL}(f_{1,\theta}(\cdot|O) \| f_{0,\theta}(\cdot|O)),$$

where the last equality denotes the average Kullback–Leibler divergence under the stationary distribution π_1 . Similarly,

$$\mu_0(\theta) = \mathbb{E}_{0,\theta}[Z_t] = -\text{KL}(f_{0,\theta}(\cdot|O) \| f_{1,\theta}(\cdot|O)) < 0.$$

Since the chain is ergodic under each hypothesis, the strong law of large numbers for Markov chains gives

$$\frac{S_n}{n} \xrightarrow[n \rightarrow \infty]{\text{a.s.}} \mu_1(\theta) \quad \text{under } H_1,$$

and

$$\frac{S_n}{n} \xrightarrow[n \rightarrow \infty]{\text{a.s.}} \mu_0(\theta) \quad \text{under } H_0.$$

Under H_1 , the process S_n grows approximately linearly with drift $\mu_1(\theta)$. Ignoring the overshoot when S_N first crosses a boundary, the time to reach the upper boundary $\log B$ is roughly

$$N \approx \frac{\log B}{\mu_1(\theta)}.$$

Taking expectations on both sides yields $\mathbb{E}_1[N] \approx \frac{|\log B|}{\mu_1(\theta)}$ (note $\log B > 0$).

Under H_0 , the process drifts downward with slope $\mu_0(\theta) < 0$. The time to hit the lower boundary $\log A$ (with $\log A < 0$) is approximately

$$N \approx \frac{\log A}{\mu_0(\theta)} = \frac{|\log A|}{|\mu_0(\theta)|},$$

hence $\mathbb{E}_0[N] \approx \frac{|\log A|}{|\mu_0(\theta)|}$.

Therefore, under the conditions of stationarity, ergodicity, and negligible overshoot, the expected sample numbers are well approximated by the expressions in (24). \square

Remark 1. The drift rates $\mu_1(\theta)$ and $\mu_0(\theta)$ are exactly the stationary Kullback–Leibler divergences between the transition laws. For i.i.d. observations, the Markov dependence vanishes and the lemma reduces to Wald’s classical ASN formulas. In practice, the approximation is accurate when the boundaries are sufficiently far from the starting point (i.e., when α and β are small).

E. Proof of InfoNCE upper-bound

Theorem 3 (InfoNCE upper-bound by information drift). *Let $P := T_{\phi\#}f_{1,\theta}$ and $Q := T_{\phi\#}f_{0,\theta}$ on \mathcal{Y} . Consider the sampling scheme: draw $J \sim \text{Unif}\{1, \dots, K\}$, then $Y_J \sim P$ and $(Y_i)_{i \neq J} \stackrel{i.i.d.}{\sim} Q$, independently of J . For any score $h : \mathcal{Y} \rightarrow \mathbb{R}$, define the InfoNCE loss*

$$\mathcal{L}_{\text{NCE},K}(h) := -\mathbb{E} \left[\log \frac{e^{h(Y_J)}}{\sum_{i=1}^K e^{h(Y_i)}} \right].$$

Then, for every $K \geq 2$,

$$-\mathcal{L}_{\text{NCE},K}(h) \leq \text{KL}(P\|Q) - \log(K). \quad (25)$$

Proof. Let $r(y) := \frac{dP}{dQ}(y)$ and write $\mathbf{Y} := (Y_1, \dots, Y_K)$. By Bayes’ rule, the posterior distribution of J given \mathbf{Y} is

$$\pi^*(j \mid \mathbf{Y}) = \frac{\mathbb{P}(J=j, \mathbf{Y})}{\sum_{i=1}^K \mathbb{P}(J=i, \mathbf{Y})} = \frac{r(Y_j)}{\sum_{i=1}^K r(Y_i)}. \quad (26)$$

The Bayes-optimal multiclass log-loss is

$$\mathcal{L}^* := \mathbb{E}[-\log \pi^*(J \mid \mathbf{Y})] = \mathbb{E} \left[\log \sum_{i=1}^K r(Y_i) \right] - \mathbb{E}[\log r(Y_J)]. \quad (27)$$

With Lemma 4, the cross-entropy with any model is no smaller than the Bayes risk, which means

$$\mathcal{L}_{\text{NCE},K}(h) \geq \mathcal{L}^* \quad (28)$$

holds for all h , and by using Bayes’ rule and the uniform prior $\mathbb{P}(J=j) = 1/K$, we have

$$I(J; Y) = \mathbb{E} \left[\log \frac{\mathbb{P}(J \mid Y)}{\mathbb{P}(J)} \right] = \mathbb{E}[\log \pi^*(J \mid Y)] - \log(1/K) = \log K - \mathbb{E}[-\log \pi^*(J \mid Y)] = \log K - \mathcal{L}^* \quad . \quad (29)$$

We have the marginal with Lemma 5:

$$\frac{d\mathbb{P}_{\mathbf{Y}}}{dQ^{\otimes K}}(\mathbf{y}) = \frac{1}{K} \sum_{i=1}^K r(y_i). \quad (30)$$

With J uniform,

$$I(J; \mathbf{Y}) = \mathbb{E} \left[\log \frac{\pi^*(J \mid \mathbf{Y})}{1/K} \right] = \mathbb{E}[\log r(Y_J)] - \mathbb{E} \left[\log \sum_{i=1}^K r(Y_i) \right] + \log K. \quad (31)$$

The first term equals the KL divergence because $Y_J \sim P$ marginally:

$$\mathbb{E}[\log r(Y_J)] = \mathbb{E}_P[\log \frac{dP}{dQ}(y)] = \text{KL}(P\|Q). \quad (32)$$

For the second term, non-negativity of KL yields

$$0 \leq \text{KL}(\mathbb{P}_{\mathbf{Y}} \| Q^{\otimes K}) = \mathbb{E}_{\mathbf{Y}} \left[\log \frac{d\mathbb{P}_{\mathbf{Y}}}{dQ^{\otimes K}}(\mathbf{Y}) \right] = \mathbb{E} \left[\log \frac{1}{K} \sum_{i=1}^K r(Y_i) \right] = \mathbb{E} \left[\log \sum_{i=1}^K r(Y_i) \right] - \log K, \quad (33)$$

which indicates $\log K - \mathbb{E}[\log \sum_i r(Y_i)] \leq 0$. Then substituting (32) and (33) into (31) gives $I(J; \mathbf{Y}) \leq \text{KL}(P\|Q)$.

Finally, by (28) and (29),

$$-\mathcal{L}_{\text{NCE}, K}(h) \leq I(J; \mathbf{Y}) - \log K \leq \text{KL}(P\|Q) - \log K.$$

□

Corollary 1 (Loss to projected KL). *For fixed-form T_ϕ , decreasing $\mathcal{L}_{\text{NCE}}(\theta, \phi)$ increases a valid lower bound to $\Phi_T(\theta, \phi)$.*

F. Proof of advantage over static test

Theorem 4 (Decreasing Loss leads to larger drifts and smaller expected samples). *Fix error budgets (α, β) . Consider the SPRT based on the true LLR increments ℓ_θ . Let (θ^*, ϕ^*) minimize $\mathcal{L}_{\text{NCE}}(\theta, \phi)$ over an admissible set. Then:*

1. $\Phi_T(\theta^*, \phi^*) \geq \Phi_T(\theta_0, \phi^*)$, hence by DPI

$$\text{KL}(f_{1,\theta^*} \| f_{0,\theta^*}) \geq \Phi_T(\theta^*, \phi^*) \geq \Phi_T(\theta_0, \phi^*).$$

2. *If, in addition, the statistic family T_ϕ is rich enough that for every $\delta > 0$ there exists $\phi = \phi(\delta)$ with $\Phi_T(\theta_0, \phi) \geq \text{KL}(f_{1,\theta_0} \| f_{0,\theta_0}) - \delta$, then for the minimizer (θ^*, ϕ^*) we have*

$$\mu_1(\theta^*) \geq \mu_1(\theta_0) - \delta,$$

and analogously for $|\mu_0|$. In particular, for arbitrarily small δ , the drifts are (weakly) increased.

3. *By Wald's relations (7) and SPRT optimality, the expected sample sizes $E_1[N]$ and $E_0[N]$ (at the same (α, β)) are (weakly) decreased.*

Proof. (1) follows from Theorem 3 and Corollary 1. For (2) apply Lemma 3 at θ_0 : for any $\delta > 0$ there exists a (finite) partition T_δ such that $\text{KL}(f_{1,\theta_0} \| f_{0,\theta_0}) \leq \text{KL}(T_\delta \# f_{1,\theta_0} \| T_\delta \# f_{0,\theta_0}) + \delta$. If the parametric family T_ϕ is dense w.r.t. this partition topology (e.g. neural universal approximation in L^1 ; see Remark 3), we can pick ϕ^* with $\Phi_T(\theta_0, \phi^*) \geq \text{KL}(T_\delta \# f_{1,\theta_0} \| T_\delta \# f_{0,\theta_0}) - \epsilon$, and let $\epsilon \rightarrow 0$. Then

$$\mu_1(\theta^*) \geq \Phi_T(\theta^*, \phi^*) \geq \Phi_T(\theta_0, \phi^*) \geq \text{KL}(f_{1,\theta_0} \| f_{0,\theta_0}) - \delta.$$

The statement for $|\mu_0|$ is identical by swapping roles of H_0, H_1 . Finally (3) follows from (7) and the SPRT optimality of expected sample size at the given (α, β) (Wald, 1992). □

Remark 2 (On separating generator and statistic parameters). It is often convenient to write $\Phi(\theta, \phi) = \text{KL}(T_\phi \# f_{1,\theta} \| T_\phi \# f_{0,\theta})$ with θ controlling the index (thus the observation laws) and ϕ controlling the statistic. In implementations one may tie them ($\phi = \theta$); the proof above treats (θ, ϕ) jointly and only requires the *form* of T_ϕ to be fixed.

Remark 3 (Approximation richness). Universal approximation (Cybenko, 1989) results imply that parametric families of measurable maps (neural networks, piecewise-constant partitions, histogram features) are dense in L^1 on compact domains. Together with lower semicontinuity of f -divergences (Sason & Verdú, 2015), this justifies the δ -tightening in Theorem 3.

Lemma 7 (SPRT is optimal in expected length at same (α, β)). *For any θ and any competing (possibly fixed-length) test achieving (α, β) , the SPRT (with the same (α, β)) satisfies*

$$E_1[N]_{\text{SPRT}, \theta} \leq E_1[N]_{\text{any}, \theta}, E_0[N]_{\text{SPRT}, \theta} \leq E_0[N]_{\text{any}, \theta}.$$

In particular $E_b[N]_{\text{SPRT}, \theta} \leq n_{\text{static}}^*(\alpha, \beta; \theta)$ for $b \in \{0, 1\}$.

Proof. This is the classical optimality of the SPRT due to Wald and Wolfowitz (see (Wald & Wolfowitz, 1948)). \square

Lemma 8 (Existence of θ_0 and a.s. equivalence to static). *Suppose the following assumptions hold and $N \geq K$:*

1. *Scoring uses s_{cos} and Φ is a deterministic top- K map. Any tie events have zero Q_b -probability and are resolved by a fixed rule.*
2. *For $b \in \{0, 1\}$, $\mathbb{P}_{q \sim Q_b}(c_K(q) > 0) = 1$.*
3. *Let \bar{Q}_b be the law of \hat{q} under H_b , and $\bar{Q} := \frac{1}{2}(\bar{Q}_0 + \bar{Q}_1)$. The support $\text{supp}(\bar{Q})$ is contained in some closed hemisphere of \mathbb{S}^{d-1} . Equivalently, the polar set is nonempty:*

$$\mathcal{U}_{\text{cos}} := \left\{ \hat{u} \in \mathbb{S}^{d-1} : \sup_{v \in \text{supp}(\bar{Q})} \langle \hat{u}, v \rangle \leq 0 \right\}$$

Then there exists θ_0 with $E_{\text{pot}}(\theta_0) = \{u_j\}_{j=1}^P$ satisfying $\hat{u}_j \in \mathcal{U}_{\text{cos}}$ for all j , such that for $b \in \{0, 1\}$,

$$\mathbb{P}_{q \sim Q_b} \left(\max_{1 \leq j \leq P} \langle \hat{q}, \hat{u}_j \rangle < c_K(q) \right) = 1 \implies f_{b, \theta_0} = f_b^{\text{static}},$$

i.e., under θ_0 the honeypots almost surely never enter the top- K and the induced observation law equals the static (documents-only) law.

Proof. If $\hat{u}_j \in \mathcal{U}_{\text{cos}}$ then for any $\hat{q} \in \text{supp}(\bar{Q})$, $\langle \hat{q}, \hat{u}_j \rangle \leq 0$; by assumption, $c_K(q) > 0$ almost surely. Hence $\max_j \langle \hat{q}, \hat{u}_j \rangle \leq 0 < c_K(q)$ almost surely, so top- K coincides with the documents-only top- K almost surely. Deterministic Φ implies equality of the induced laws. \square

Theorem 5 (Loss-minimizing training improves the operational goal over the static optimal). *There exist untrained parameter θ_0 make vector database equivalent to vector database without honeypots and θ^* the post-training parameter obtained by minimizing \mathcal{L}_{NCE} . Under the assumptions of Theorem 4, for the same (α, β) , and $b \in \{0, 1\}$,*

$$E_b[N]_{\text{SPRT}, \theta^*} \leq \min \left\{ E_b[N]_{\text{SPRT}, \theta_0}, E_b[N]_{\text{any, static}} \right\},$$

with strict inequality whenever the drifts increase strictly.

Proof. By Lemma 8, there exists θ_0 under assumptions such that $f_{b, \theta_0} = f_b^{\text{static}}$ for $b \in \{0, 1\}$. Hence the SPRT at (α, β) under θ_0 has expected sample size equal to the static optimal with Lemma 7. By Theorem 4, the drifts $\mu_1(\theta), |\mu_0(\theta)|$ (weakly) increase after training, hence the Wald relations (7) imply (weakly) smaller $E_b[N]$ for the SPRT at (α, β) , and $\mu_b(\theta) \geq \mu_b(\theta_0)$ holds by letting $\delta \rightarrow 0$. Combine all have the inequality. \square

G. Algorithm of Scorer Guided embedding inversion

Scorer guided beam-search embedding inversion algorithm (Zhang et al., 2025) is shown below:

Algorithm 1 Embedding Inversion

Hyperparameters: beam width b , top- k
Input: prefix prompt P , target embedding $\mathbf{e}_{\text{target}}$
Output: best found sequence of length max_length

```
1: Initialize: Beams  $\mathcal{B} = \{\text{empty string}\}$ 
2: for each time step  $t$  from 1 to  $\text{max\_length}$  do
3:    $\mathcal{B}_{\text{new}} \leftarrow \{\}$ 
4:    $\mathcal{S}_{\text{new}} \leftarrow \{\}$ 
5:   for each beam  $b \in \mathcal{B}$  do
6:      $z_t \leftarrow \text{LLM}_{\text{logits}}(P \oplus b)$ 
7:      $\text{topk\_tokens} \leftarrow \text{TopK}(z_t, k)$ 
8:     for each token  $t_k \in \text{topk\_tokens}$  do
9:        $b' \leftarrow b \oplus t_k$ 
10:       $\mathcal{B}_{\text{new}}.\text{append}(b')$ 
11:       $\mathcal{S}_{\text{new}} \leftarrow \text{Scorer}(\mathcal{B}_{\text{new}}, \mathbf{e}_{\text{target}}, S, \mathcal{E}_{\text{doc}})$ 
12:    end for
13:   end for
14:   Sort  $\mathcal{B}_{\text{new}}$  by  $\mathcal{S}_{\text{new}}$ 
15:    $\mathcal{B} \leftarrow \mathcal{B}_{\text{new}}[:b]$ 
16: end for
17: return  $\mathcal{B}[0]$ 
```

H. Examples of Honeypot Documents

We provide a few honeypot documents example here, corresponding to WebShop, Pokémon and Healthcare scenarios respectively:

Honeypot Documents Example

Pot 1: “Web Shopping: **1432**: With just six keywords like search term in 'search: []'; there already comes together several possibilities within three of which all work or more (inclusu[.]m any other product to find them for sure without searching again from memory alone as this will get out”

Pot 2: “Alright, Nature offers an enchanting and unique array of creatures with incredible strength! A rare breed from Japan - Pokémon that has the physical properties described below: * Name – P.E”

Pot 3: “Creating concise passages from this resource while generating appropriate dialogue within my parameters where all data needs filtering every fourth point but those facts/assums or ”sugar-crate-loads The patient reports experiencing various physical discomforts and functional changes.”